Incorporation of Lithium by MgH2: An Ab Initio Study

ARTICLE *in* THE JOURNAL OF PHYSICAL CHEMISTRY C · NOVEMBER 2013

Impact Factor: 4.77 · DOI: 10.1021/jp404993z

THE JOURNAL OF PHYSICAL CHEMISTRY C

Article

pubs.acs.org/JPCC

Incorporation of Lithium by MgH_2: An Ab Initio Study

D. Meggiolaro,[†,‡] G. Gigli,[†] A. Paolone,[‡] F. Vitucci,[‡] and S. Brutti*[,‡,§]

[†]Dipartimento di Chimica, Sapienza Università di Roma, 00185 Rome, Italy

[‡]Istituto dei Sistemi Complessi, Consiglio Nazionale delle Ricerche (ISC−CNR) UOS Sapienza, 00185 Rome, Italy

[§]Dipartimento di Scienze, Università della Basilicata, 85100 Potenza, Italy

Supporting Information

ABSTRACT: The incorporation of lithium by MgH_2 through an electrochemical conversion reaction is a valuable alternative to Li intercalation into graphite for next-generation Li-ion cells. The incorporation of lithium occurs by the reduction of magnesium hydride to magnesium metal nanoparticles surrounded by an amorphous matrix of lithium hydride. In this study we present a computational investigation of the conversion reaction of MgH_2 to give Mg and LiH by first-principles methods. Density functional theory calculations have been performed using plane waves and projector augmented wave (PAW) pseudopotentials within the generalized-gradient approximation by the VASP code. The existence of intermediate phases has been checked by finite temperature ab initio thermodynamic calculations. Also, the occurrence of solid solutions in the first stages of lithium incorporation has been studied by the supercell approach by predicting their thermodynamic stability at 0 K. Five different solid solutions have been mimed by forming 0D defects in the MgH_2 lattice: (a) vacancies in the hydride sites; (b) interstitial lithium insertion; (c) substitution of lithium in hydride sites; (d) substitution of lithium in magnesium sites; (e) substitution of lithium in magnesium sites with parallel formation of vacancies in the hydride sites. Preliminary results about the thermodynamics of the conversion reaction in nanometric MgH_2 clusters are also discussed.

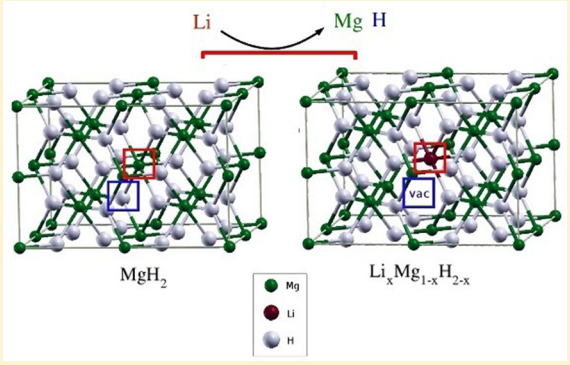

1. INTRODUCTION

The incorporation of lithium by MgH_2 through an electrochemical conversion reaction is a promising alternative to Li intercalation into graphite for next-generation Li-ion cells. In fact MgH_2 has a theoretical capacity of 2048 mAh g^{-1} to be compared to 372 mAh g^{-1} of graphite. Its ability to reversibly incorporate/deincorporate lithium in an electrochemical lithium cell has been verified experimentally by Aymard and co-workers and by us in recent years.[1−4] The incorporation of lithium in a MgH_2-based electrode occurs by the reduction of magnesium hydride to magnesium metal nanoparticles surrounded by an amorphous matrix of lithium hydride. This kind of electrochemical process is a hydride conversion reaction (HCR): such a process has been proposed in 2008 by Tarascon and co-workers[2] for high capacity Li-ion cell electrodes. In general conversion reactions occur starting from a large variety of possible inorganic phases such as oxides, nitrides, phosphides, fluorides, and sulfides:[5] their exploitation in full Li-ion cells has been already illustrated in the literature, as an example in the case of iron oxide.[6] The main advantage of conversion reaction materials is their ability to exchange more than one electron per redox center. Depending on the oxidation state of the metal, these reactions have been reported to involve one (Cu_2O), two (MnO), three (Fe_2O_3), or four (RuO_2) electrons. More recently Boyanov et al.[7] observed that anions may also take part in a conversion reaction when the metal ions are covalently bonded to their surrounding ligands. As a consequence innovative conversion electrodes can be developed with outstanding capacity improvements over graphite or insertion oxides. The occurrence of a reversible HCR on MgH_2-based electrodes in lithium cells has been already verified by ex situ X-ray diffraction (XRD) and electron microscopy investigations.[1,2] However the reaction mechanism has been simply sketched, and the occurrence of initial or extended solid solutions or the formation of intermediate phases cannot be excluded. Moreover, only nanometric MgH_2 powders are apparently able to exchange Li ions in a cell, whereas bulk MgH_2 seems electrochemically inactive. In a previous paper[1] we reported that MgH_2 XRD peaks shift upon electrochemical lithium incorporation leading to an apparent lattice contraction. From a general point of view upon electrochemical lithium incorporation two different phenomena may occur: the nucleation of a new phase with similar or different structure or a limited lithium insertion into the MgH_2 lattice. It should be noted that the nucleation of a new phase may lead to rather different XRD patterns than the formation of a lithiated Li_xMgH_2 solution phase. On the other hand a shift of the Bragg peak is likely explained by the second mechanism.

Received: May 21, 2013
Revised: September 16, 2013
Published: September 17, 2013

   dx.doi.org/10.1021/jp404993z | J. Phys. Chem. C 2013, 117, 22467−22477

Table 1. Summary of the Reactions: a) the Overall Conversion Reaction and Mechanical Demixing Reactions for Suggested Phases $LiMgH_3$ and Li_2MgH_4 and b) Proposed Reactions for Insertium Mechanism of Li in MgH_2 in the First Stages of the HCR

(a) Line compounds reactions		
$MgH_2 + 2Li \rightarrow 2LiH + Mg$	(R1)	HCR
$LiMgH_3 \rightarrow LiH + MgH_2$	(R2)	demixing reaction
$Li_2MgH_4 \rightarrow 2LiH + MgH_2$	(R3)	demixing reaction
(b) Solid solutions reactions		
$xLi + MgH_2 \rightarrow MgH_{2-x} + xLiH$	(R4)	H vacancy formation
$xLi + MgH_2 \rightarrow Li_xMg_{1-x}H_2 + xMg$	(R5)	Mg substitution
$xLi + MgH_2 \rightarrow Li_xMgH_2$	(R6)	Interstitial solid solution
$2xLi + MgH_2 \rightarrow Li_xMgH_{2-x} + xLiH$	(R7)	H substitution
$2xLi + MgH_2 \rightarrow Li_xMg_{1-x}H_{2-x} + xMg + xLiH$	(R8)	Mg substitution and H vacancy formation

However, due to the strongly covalent Mg−H bonds in MgH_2, the simple insertion of Li into MgH_2 is not expected to have a contraction effect on the unit cell parameters. Bond contractions generally occur when Li^+ incorporation induces a large screening effect on the repulsive anion−anion interactions: this condition is not trivially obvious in the case of MgH_2 and requires investigation. Furthermore, the overall conversion process occurs with large volume expansion and apparent sintering among magnesium nanoparticles: these effects can be clues of a more complex reaction path compared to the simple HCR. This is even more important considering that, as already discussed, "going-nano" plays a key role in the promotion of the MgH_2 HCR. This last effect can be thermodynamic and/or kinetic as it may involve variation of the chemical potentials of nanophases as well as drastic improvements in the ion diffusivity, due to shorter diffusion paths across particles.

The formation of Li−Mg−H ternary phases has never been experimentally verified and reported in the literature. As an example, in an experimental study about the synthesis of perovskite-like $Li_xNa_{1-x}MgH_3$ mixed hydride by ball milling from LiH, NaH, and MgH_2, Ikeda et al.[8] did not observe the formation of a single phase at $x = 1$, i.e., $LiMgH_3$. From the computational side Chen et al.[9] recently predicted by first-principles methods that two lithium magnesium mixed hydrides, namely, Li_2MgH_4 and $LiMgH_3$, are thermodynamically stable at 300 K. Their predicted ground-state structures are $NaMg_2Cl_4$-type and $LiTaO_3$-type, respectively. On the contrary previous lattice stability studies at 0 K by Pfrommer et al.[10] and Vajeeston et al.[11] for the $LiMgH_3$ stoichiometry found that this composition is slightly unstable with respect to demixing into pure hydrides ($LiH + MgH_2$) either starting from perovskite-like ($CaTiO_3$-like), ilmenite-like ($FeTiO_3$), or the above-mentioned rhombohedral $LiTaO_3$-like prototype lattices. Recently, Smith et al.[12] studied the dopant-vacancy coupling in Li-doped magnesium hydrides by first-principle methods using supercells. They found that Li-doped MgH_2 is thermodynamically metastable with respect to phase separation into pure MgH_2 and LiH, apparently at any significant Li concentration. Concerning the effect of nanometrization, many authors verified, both theoretically and experimentally, that the reduction of MgH_2 particle size to the nanoscale promotes the hydrogen release at moderate temperatures by tuning up the desorption thermodynamics.[13−18] It is likely that similar effects can play a role also in the case of room-temperature HCR processes in Li cells.

Conversion reactions in lithium cells have been studied by first-principles by Doublet and co-workers in the case of phosphides[19] and oxides.[20] In particular Doublet et al. focused on the study of the multiple interphases ($M_aX_b/M/Li_{2b/a}X$) to understand the origin of the voltage hysteresis upon cycling in real cells. In this study we present a computational investigation of the conversion reaction of MgH_2 to give Mg and LiH by first-principles methods. Apparently our study is the first ever reported computational investigation of a HCR process. Density functional theory calculations have been carried out using plane waves and pseudopotentials within the generalized-gradient approximation by the VASP code and the PHONOPY routines. A general summary of the reactions studied is presented in Table 1. The existence of intermediate phases $LiMgH_3$ and Li_2MgH_4 in the (MgH_2−Mg + 2LiH) pseudobinary system has been checked by finite temperature ab initio thermodynamic calculations studying their thermodynamics stability (see reactions R2 and R3 in Table 1). The 0 K energetics and the phonon dispersions have been predicted to calculate the Gibbs energy of formation at 300 K.

Furthermore, the occurrence of solid solutions in the first stages of lithium incorporation (reactions R4−R8 in Table 1) has been studied by the supercell approach, by predicting their thermodynamic stability at 0 K. Five different solid solutions have been modeled by forming 0 D defects in the MgH_2 lattice: (R4) vacancies formation in the hydride sites; (R5) substitution of lithium in magnesium sites; (R6) interstitial lithium insertion; (R7) substitution of lithium in hydride sites; (R8) substitution of lithium in magnesium sites with parallel formation of vacancies in the hydride sites. The configuration entropy has been evaluated for each solid solution, and the Gibbs reaction energies at 300 K have been calculated for the formation of all five solid solutions from MgH_2 and Li. In addition, in the last section of this article preliminary results about the thermodynamics of the conversion reaction in a large MgH_2 cluster are also discussed.

2. COMPUTATIONAL DETAILS

2.1. Setting Exchange-Correlation Functional and Pseudopotentials. Calculations have been performed by density functional theory (DFT), using plane wave (PW)[21] basis sets as implemented in the VASP code.[22] To set both exchange-correlation functional and pseudopotentials, a system-

dx.doi.org/10.1021/jp404993z | J. Phys. Chem. C 2013, 117, 22467−22477

atic study of equilibrium structural properties of bulk phases involved in reaction R1 (e.g., LiH, Li, Mg, and MgH_2) has been performed, testing different combinations. All these phases, being well-known, are good benchmarks to test the reliability of our computational approach, for either the exchange-correlation or the interactions between semicore and valence electrons.

Equilibrium lattice constants and cohesive energies of these systems have been calculated and compared with experiments. Results are reported in Table S1 (Supporting Information). Optimized structures and energies have been converged to an energy cutoff of 450 eV and a 10 × 10 × 10 Monkhorst−Pack (MP) grid with a final computational accuracy better than 1 meV/at. Structures have been relaxed down to a convergence threshold of 10^{-4} eV/Å on forces. To compare the calculated cohesive energies of Li, LiH, and MgH_2 with available experimental data, spin-polarized energies of isolated atoms (e.g., H and Li atoms) have been used. All pseudopotentials tested describe interactions between core and valence electrons within the projector augmented wave (PAW)[23] method keeping all core electrons frozen.

As expected remarkable differences between computational results and experimental data are observed for LDA predictions. A better agreement can be achieved using a generalized gradient approximation (GGA):[24,25] apparently both the GGA functionals by Perdew−Wang (PW91)[24] and Perdew−Burke−Ernzerhof (PBE)[25] give very similar satisfactory results. This trend is also confirmed for the calculated direct band gaps of MgH_2 and LiH derived by the typical minimal energy difference between the HOMO and LUMO in the band structure at constant k-point (vertical transition).[26] LDA values of 4.5 and 2.6 eV have been found for MgH_2 and LiH, respectively, to be compared with the 4.8 and 3.0 eV calculated in the GGA-PW91 approximation. As expected these predictions fail an accurate reproduction of the experimental optical band gaps, the latter being 5.6[27] and 4.9 eV[28] for MgH_2 and LiH, respectively. However, although GGA approximation allows a slightly better estimate compared with a local density description, it should be pointed out that the underestimation of band gap is a well-known issue of the DFT framework.

For what concerns the role of semicore states for Li and Mg, the adoption of larger basis (i.e., 1s and 2s2p states for Li and Mg, respectively) apparently does not lead to major effects on the accuracy of both the structure and energetic predictions of the MgH_2, Li, Mg, and LiH phases (see Table S1, Supporting Information).

In the light of these preliminary tests on Li, Mg, LiH, and MgH_2, all our DFT calculations reported in the followings have been performed within the generalized gradient approximation described by the Perdew and Wang (PW91) functional employing PAW pseudopotentials. Only valence electrons in the variational basis have been used, to reduce the computational effort. By this approach, DFT predictions for Mg, Li, LiH, and MgH_2 agree with experimental values within 3% for the cohesive energies and 1.5% for the lattice constants.

2.2. Line Compounds and Metals. Total energies of line compounds in reactions R1−R3 have been calculated using a kinetic energy cutoff of 450 eV and a common uniform 10 × 10 × 10 Monkorst−Pack grid reaching a computational accuracy of 2 meV/atom. Structures have been fully relaxed: the final threshold on forces has been set to 2 × 10^{-4} eV/Å on each atom. Phonon dispersions have been calculated in harmonic approximation by the small displacement method (SDM) using PHONOPY.[29] In this approach a large portion of the considered system is reproduced by a supercell, and the Hellmann−Feynman forces acting on each atom of the supercell after a single atom displacement are determined by simple DFT runs. This scheme allows us to build the dynamical matrix that can be further diagonalized to estimate eigenfrequencies of the system. This is done automatically by the PHONOPY routines, while forces acting on each atom are calculated self-consistently by the VASP package. To calculate correctly forces acting on atoms, atomic displacements in each direction in the supercell have been set equal to 0.015 Å. The thermodynamic properties of line compounds have been calculated by the usual equations

$$S_{vib}(T) = -k_B \sum_{\mathbf{q},s} \ln[1 - \exp(-\hbar\omega(\mathbf{q}, s)/k_B T)] - \frac{1}{T} \sum_{\mathbf{q},s} \frac{\hbar\omega(\mathbf{q}, s)}{\exp(\hbar\omega(\mathbf{q}, s)/k_B T) - 1} \quad (1)$$

$$H_{vib}(T) = \sum_{\mathbf{q},s} \frac{1}{2}\hbar\omega(\mathbf{q}, s) + \frac{\hbar\omega(\mathbf{q}, s)}{[\exp(\hbar\omega(\mathbf{q}, s)/k_B T) - 1]} \quad (2)$$

where $S_{vib}(T)$ and $H_{vib}(T)$ are vibrational entropy and enthalpy respectively; $\omega(\mathbf{q}, s)$ represents vibration frequency at $\mathbf{q}$ point of band index s; k_B is the Boltzmann constant; and T is the temperature. The $\Delta_f G(T)$ for each phase has been determined according to the general expression

$$\Delta_f G(T) = \Delta_f E_{el} + \Delta_f ZPE + \Delta_f H_{vib}(T) - T\Delta_f S_{vib}(T) \quad (3)$$

where E_{el} is the electronic energy as calculated from DFT; ZPE is the zero point vibrational energy (i.e., the first term on the RHS of eq 2); and $H_{vib}(T)$ and $S_{vib}(T)$ are the enthalpy and entropy at temperature T, respectively.

2.3. Solid Solutions. Energetics of reactions R4−R8, involving defective lattices, have been studied using the supercell approach, starting from the unperturbed MgH_2 lattice. The size of the supercells has been varied to mimic different values of defect concentrations (x). Within this approach only one point (0 D) defects are considered: 2 × 2 × 2, 2 × 2 × 3, and 3 × 3 × 4 supercells have been employed to model all defective systems.

Spin-polarized DFT calculations have been performed using the spin interpolation formula of Vosko et al.[30] with a uniform energy cutoff of 450 eV and two sets of k points in BZ: a uniform MP mesh of 2 × 2 × 2 points for the 2 × 2 × 2 and 2 × 2 × 3 supercells and the only gamma point for the 3 × 3 × 4 supercell. By these sets of parameters a computational accuracy on the total energy of 2 meV/atom can be achieved. Structures have been fully relaxed: the threshold on forces has been set to 0.01 eV/Å.

The defect formation energy (DFE) for neutral impurities is defined as[31]

$$DFE = E_{tot}(X) - E_{tot}(0) + \sum_i n_i \mu_i \quad (4)$$

where $E_{tot}(X)$ is the total energy of the defective lattice supercell with impurity specie X; $E_{tot}(0)$ is the energy of the nondefective lattice supercell; and the last term corresponds to the sum of the number of atoms entering ($n_i < 0$) or leaving ($n_i > 0$) the perfect lattice during the defect formation reaction

dx.doi.org/10.1021/jp404993z | J. Phys. Chem. C 2013, 117, 22467−22477

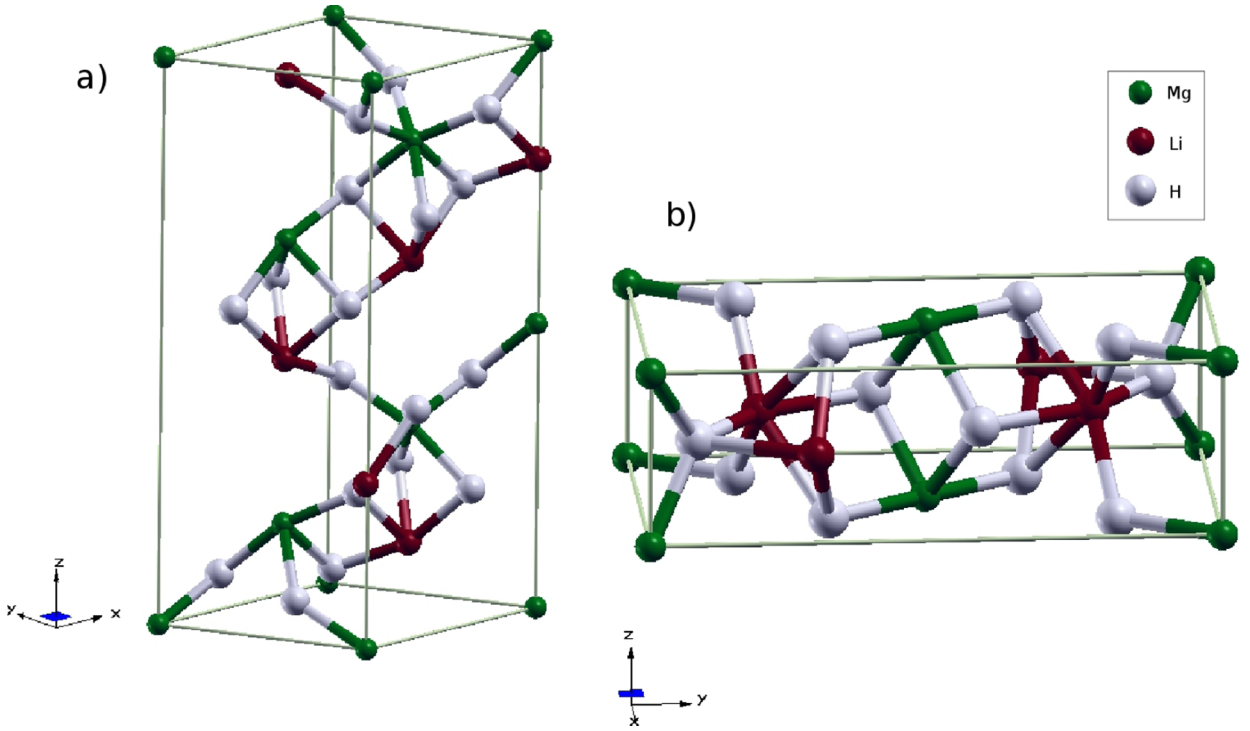

Figure 1. Optimized structures of (a) $LiMgH_3$ and (b) Li_2MgH_4. Values of the lattice constants are reported in Table 2.

multiplied by the chemical potential of the respective reservoir. The chemical potentials of the reservoirs have been set to the respective bulk values for Mg and Li and to the gas-phase H_2 for H atoms.

Configurational entropy in defective systems has been calculated at $T = 0$ K using the Boltzmann equation

$$S_{conf} = k_B \ln \frac{N!}{n!(N-n)!} \quad (5)$$

where n is the number of defects and N is the number of atomic sites in the supercell equivalent to the defective one or, in the case of interstitial disorder, the overall number of equivalent interstitial sites in the supercell considered. Considering only one defect for each supercell, all the possible substitutions become equivalent. Hence, a microcanonical ensemble fully describes the configurational entropy of the system, and eq 5 becomes $S_{conf} = k_B \ln N$.

Energetics of reactions R4−R8 has been reported as $\Delta_r E(0\ K)$ and, by adding configurational entropies, as $\Delta_r G(300\ K)$ according to eq 5. Vibrational contributions for supercells have been neglected: this assumption reasonably has minor effects on the predictions of reaction thermodynamics in the view of the foreseen compensations between reagents and products in the final estimates.

2.4. Clusters. To study surface effects on the R4−R8 reaction thermodynamics, preliminary DFT calculations have been also performed on stoichiometric and defective clusters of MgH_2.

Clusters have been created cutting a sphere of radius 5 Å from the MgH_2 bulk and saturating with H atoms all Mg atoms on the surface to preserve stoichiometry. Hydrogen atoms have been bonded on these sites accordingly to a minimum symmetry loss requirement with respect to the original MgH_2 bulk phase. In particular, starting from a nonstoichiometric $Mg_{31}H_{60}$ cluster cut from the bulk that retains all point symmetry operations of the bulk phase (i.e., D_{2h}), we saturated Mg atoms on the surface with two H atoms, thus breaking down the symmetry of the cluster to C_{2v}. All the other choices that lead to less symmetric systems have been discarded.

Spin-polarized DFT calculations[30] have been performed in the PBE[25] scheme using pseudopotentials described by the PAW method.[23] Total energies of clusters were found in the supercell approach, fully relaxing ion positions until a convergence of 0.01 eV/Å on forces has been reached. To this aim, a sufficiently large cubic supercell has been used with lattice constant of 20 Å, assuring a distance between atoms of different replicas greater than 10 Å. Several tests have been performed enlarging the supercell size to achieve a total energy convergence below 2 meV/atom. The kinetic energy cutoff has been set to 400 eV; all calculations have been performed at the only gamma point.

3. RESULTS

3.1. HCR Reaction. The HCR reaction R1

$$2Li + MgH_2 \rightarrow 2LiH + Mg \quad (6)$$

is the overall reaction of the electrochemical process of conversion of MgH_2 in lithium batteries: the experimental voltage value of this reaction lays in the range 0.50−0.55 V vs Li^+/Li.[1,2]

The computational prediction of the voltage potential (ΔE^0) of reaction R1 at $T = 300$ K is easily obtained by using the general expression $\Delta E^0 = -\Delta_r G/nF$, where $\Delta_r G$ is the free Gibbs reaction energy of R1; n is the number of electrons exchanged (e.g., 2 in the case of MgH_2); and F is the Faraday constant: $\Delta_r G$ values of reaction have been calculated according to eq 3.

Total energies of optimized bulk phases Li, Mg, MgH_2, and LiH have been used to calculate $\Delta_r E$ of R1, and phonon

dx.doi.org/10.1021/jp404993z | J. Phys. Chem. C 2013, 117, 22467−22477

dispersion calculations in the SDM approximation have been performed to account for vibrational corrections.

By our approach, a negative $\Delta_r G = -104.9$ kJ/mol has been predicted corresponding to an electrochemical voltage $\Delta E^0 = 0.53$ V vs Li^+/Li at $T = 300$ K (0.55 V at $T = 0$ K), in excellent agreement with the experimental value.

3.2. $LiMgH_3$ and Li_2MgH_4 Intermediate Phases. As discussed above, the occurrence of intermediate phases in the Mg−Li−H ternary system is under debate. The study carried out by Chen et al.[9] about the lattice stability of $LiMgH_3$ and Li_2MgH_4 suggests a *R*3*c* ($LiTaO_3$-type) ground-state structure for $LiMgH_3$ and a *Pbam* (Na_2MgCl_4-type) ground state for Li_2MgH_4. Both these lattices have been predicted by Chen et al. to be thermodynamically stable showing positive $\Delta_r G°(300\ K)$ for the demixing reactions R2 and R3. Their unit cells are shown in Figure 1. On the other hand, previous less exhaustive studies by Pfommer[10] and Vajeston[11] suggest that $LiMgH_3$ lattice demixes spontaneously giving LiH + MgH_2.

We newly investigated the thermodynamic stability of the two ground-state lattices found by Cheng et al.[9] Results of the geometry optimization are reported in Table 2 compared with Chen's evaluations.

Table 2. Lattice Constants and Symmetries for Optimized $LiMgH_3$ and Li_2MgH_4[a]

system	space group	number ions	lattice constants	Chen et al.[9]
$LiMgH_3$	C_1	30 ($Z = 6$)	$a = b = 4.941$	4.9226
			$c = 13.281$	13.2106
Li_2MgH_4	*Pbam*	14 ($Z = 2$)	$a = 4.882$, $b = 9.231$	4.8968, 9.2532
			$c = 2.913$	$c = 2.9185$

[a]Also Chen et al. values for lattice constants are reported for comparison.

The $LiMgH_3$ equilibrium structure relaxes in a hexagonal cell with 30 atoms, corresponding to 6 unit formulas per cell. However, the relaxing of the *R*3*c* cell suggested by Chen never converged within our severe threshold on forces. After the breaking down of the symmetries on the atomic sites, the cell reached the required convergence on forces with a final space group C_1. In the converged structure Mg atoms are coordinated by six H atoms in a distorted octahedron with bond lengths ranging in a wide interval, i.e., 1.92−2.00 Å, and angles between 84° and 101°. Li atoms have five neighbors H atoms and Li−H bond lengths between 1.92 and 2.07 Å. These results are in agreement with Chen calculations although with different space group symmetry of the final relaxed structure.

The relaxed Li_2MgH_4 retains all the original symmetries leading to an equilibrium *Pbam* rombohedrical cell with 14 atoms, corresponding to 2 unit formulas per cell. Li and Mg atoms are both coordinated by six H atoms in distorted octahedra with bond lengths in the ranges of 1.89−2.13 and 1.94−1.95 Å for Li−H and Mg−H, respectively, in agreement with Chen findings.

Electronic structures confirm that both $LiMgH_3$ and Li_2MgH_4 are insulators with band gaps wider than 3.5 eV. Chemical bonds have a partially ionic character: the analysis of the Bader charges highlights a net charge on H atoms close to −0.8.

Starting from the optimized structures, the dynamical matrices have been calculated by the small displacement method. All the thermodynamic predictions for systems involved in reactions R1−R3 are reported in Table S2 (Supporting Information), together with the size of the supercells used to calculate phonons.

The computed $\Delta_f G(300\ K)$ values of $LiMgH_3$ and Li_2MgH_4 are negative: the final values are −142.2 and −218.5 kJ/mol for $LiMgH_3$ and Li_2MgH_4, respectively. Apparently the vibrational correction plays a marginal role: the $\Delta_f G(0\ K)$ are reported and compared to those calculated at 300 K in Table S3 in the Supporting Information. As expected, data at 0 K are slightly more negative than the values at 300 K. However, demix reactions R2 and R3 show a negative $\Delta_r G$ of −3.3 and −9.4 kJ/mol, respectively, at 300 K and of −4.2 and −12.7 kJ/mol at 0 K. This result disagrees with Chen predictions. This difference is likely due to the much more severe convergence parameters used by us on the kinetic energy cutoffs, k-point mesh, threshold on forces, and self-consistent field energies. It is to be noted that, to validate our results, we checked all our predictions using different exchange-correlation functionals and including semicore electrons in the variational basis without observing any change in the sign of both demixing reactions.

In Table 3 the electrochemical voltages and the corresponding $\Delta_{HCR}G$ for HCR reactions of $LiMgH_3$ and Li_2MgH_4 are reported at 0 K and 300 K. All the HCRs involving the hypothetical mixed hydrides show electrochemical voltages lower than the overall MgH_2 conversion potential (0.55 V at 0 K and 0.53 V at 300 K; see previous section). As a consequence the occurrence of HCR reactions involving any of the two intermediate mixed hydrides is thermodynamically excluded by the competitive overall HCR. In fact the latter shows a larger

Table 3. $\Delta_{HCR}G$ and Associated Voltages $E/E^0(Li^+/Li^0)$ for $LiMgH_3$ and Li_2MgH_4 Conversion Reactions: Values at 0 K and 300 K are Reported

HCR reaction	T	$\Delta_{HCR}G$ (kJ/mol)	E/E^0 (V)
$2MgH_2 + 2Li \rightarrow Mg + LiMgH_3$			
	0 K	−100.7	0.52
	300 K	−98.4	0.51
$2MgH_2 + 2Li \rightarrow Mg + Li_2MgH_4$			
	0 K	−92.2	0.48
	300 K	−92.3	0.48
$2LiMgH_3 + 2Li \rightarrow Li_2MgH_4 + 2LiH + Mg$			
	0 K	−100.2	0.52
	300 K	−98.9	0.51

dx.doi.org/10.1021/jp404993z | J. Phys. Chem. C 2013, 117, 22467−22477

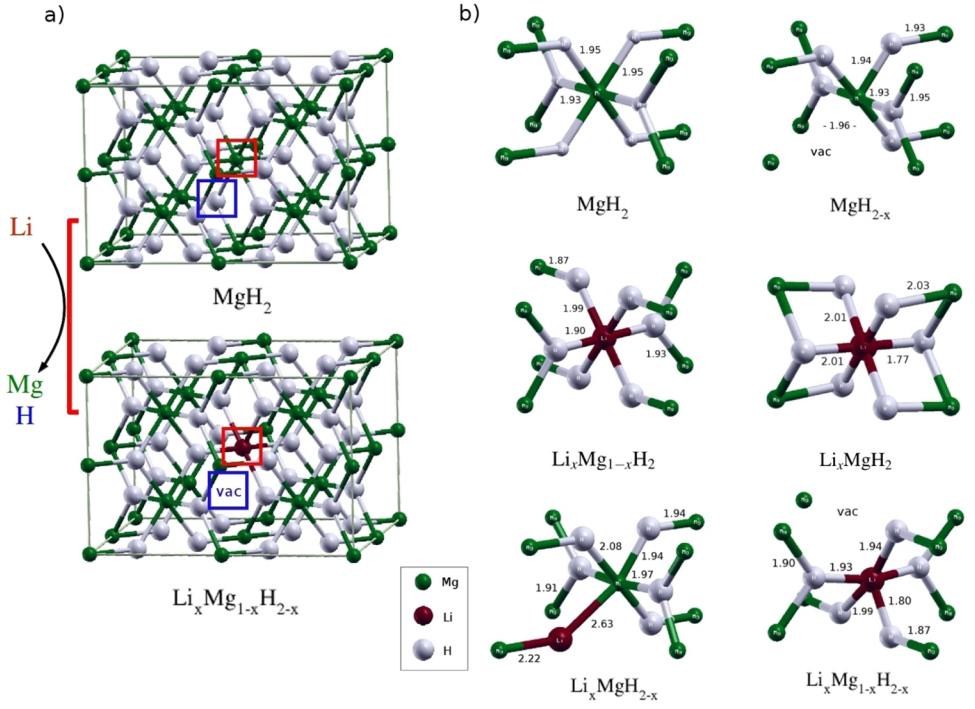

Figure 2. (a) Example of the $Li_xMg_{1-x}H_{2-x}$ modeling by the supercell method: defective sites are indicated by colored squares. (b) Calculated equilibrium structures of defect sites in all five defective systems.

Gibbs energy change at both 0 and 300 K and therefore a higher electrochemical potential. In summary, our study about the thermodynamics of the $LiMgH_3$ and Li_2MgH_4 intermediate phases predicts such lattices as metastable. They are expected to spontaneously demix to MgH_2 + LiH and therefore are unlikely to form in lithium cells during the MgH_2 HCR process.

3.3. Defective Systems. Turning to the defective systems, the occurrence of solid solutions in the first stages of Li incorporation by MgH_2 has been investigated. The five different mechanisms studied are summarized by reactions R4−R8 in Table 1. To evaluate thermodynamically these reactions, the corresponding solid solutions (i.e., defective systems) have been modeled.

DFT calculations have been performed in supercells of different sizes to model different defect concentrations: 2 × 2 × 2, 2 × 2 × 3, and 3 × 3 × 4 supercells were employed, corresponding to defect atomic molar fractions x of 0.062, 0.042, and 0.014, respectively. The atomic molar fraction x is defined here as the reciprocal of the total number of MgH_2 unit formulas in the nondefective supercells employed in the calculations: (1/16), (1/24), (1/72) for 2 × 2 × 2, 2 × 2 × 3, and 3 × 3 × 4 supercells, respectively.

MgH_2 supercells have been built making replicas in the three spatial directions of optimized crystal structure. After the reoptimization of the nondefective MgH_2 supercells, point defects have been introduced and modeled: in Figure 2a, a pictorial representation of this approach is presented. The calculated equilibrium structures of the first neighbors coordination shell around the point defects are shown in Figure 2 for all the five systems, compared to the unperturbed lattice of MgH_2.

The DFEs associated to the creation of the point defects in each defective lattice have been calculated according to eq 4 and are reported in Table 4. A comparison of the electronic density of states (DOS) of MgH_2 and the defective systems is shown in Figure 3 to highlight the electronic disorder induced in each case by the point defects.

Table 4. Calculated DFEs for the Defective Systems Involved in Reactions R4−R8[a]

system	2 × 2 × 2	2 × 2 × 3	3 × 3 × 4
MgH_{2-x}	136.0	135.7	136.5
$Li_xMg_{1-x}H_2$	231.2	222.1	233.6
Li_xMgH_2	125.4	108.4	94.4
Li_xMgH_{2-x}	331.9	336.1	348.0
$Li_xMg_{1-x}H_{2-x}$	72.6	73.4	72.5

[a]All values are reported in kJ/mol. The supercell employed for the calculation is indicated at the top.

The MgH_{2-x} system is a hydrogen defective MgH_2 lattice. The point defect has been modeled by introducing a single H vacancy in each of the three different supercells. The H vacancy formation reaction can be written in Kroger−Vink notation as $H_H^x = H_S^x + V_H^x$, in which a H atom moves from his lattice position H_H^x in the bulk to the surface H_S^x, leaving a neutral H vacancy V_H^x in the lattice. The calculated DFEs for different supercells spread in the narrow range 135.7−136.5 kJ/mol, in excellent agreement with the value found by Smith et al.[12](i.e., 135.3 kJ/mol). The structure of the empty site in the relaxed supercell is reported in Figure 2 together with the surrounding Mg−H bond lengths. The H vacancy induces a slight contraction of Mg−H bonds in the first neighbor octahedra, whereas the second coordination shell seems unaltered. Small deviations of octahedra angles from original values are also observed. The analysis of DOS suggests that the unpaired electron left by the H vacancy creates two spin oriented localized states in the middle of the MgH_2 band gap, separated by ≈0.7 eV. The spin-up occupied state is approximately 2 eV above the valence band edge, whereas the unoccupied spin-down state is very close to the conduction band. The large

dx.doi.org/10.1021/jp404993z | J. Phys. Chem. C 2013, 117, 22467−22477

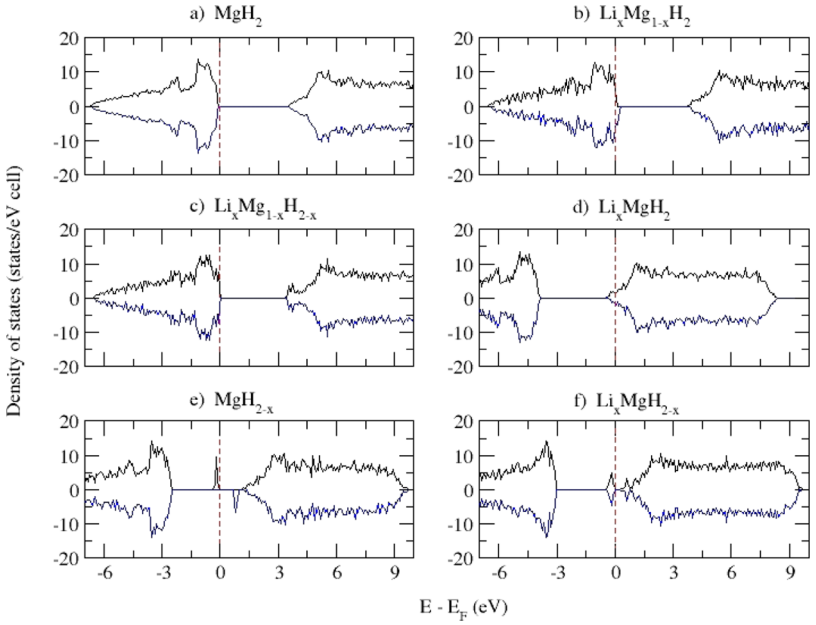

Figure 3. Calculated electronic density of states of the five defective systems: energies are scaled to the Fermi energy. Spin-up and spin-down components are indicated in black and blue, respectively.

ionization energy predicted by DFT suggests that this kind of defect is unlikely to be ionized at low temperatures.

The defective system originated by the substitution of one Mg atom by Li in the MgH_2 lattice can be described by the defect formation reaction $Li + Mg^x_{Mg} = Li^x_{Mg} + Mg_s$, where Mg^x_{Mg} and Mg_s represent the Mg atom in the MgH_2 lattice and on the surface, respectively, and Li^x_{Mg} is the substitutional Li neutral atom. The DFE of this reaction lays in the range 222.1−233.6 kJ/mol, indicating a remarkable destabilization of the MgH_2 lattice induced by Li substitutional doping on the Mg site. The Li atom in the Mg site is coordinated by six H atoms (like Mg in the pristine lattice) in an octahedral structure elongated along two out of the six Li−H bonds, of about 0.04 Å. This expansion leads to the contraction of the vicinal Mg−H bonds. The electronic DOS shows shallow spin-down unoccupied levels at the top of the valence band, indicating the presence of acceptor states typical of p-doped structures. The low ionization energy indicates that also at low temperatures this kind of defect may be ionized according to the reaction $Li^x_{Mg} = Li'_{Mg} + h^\bullet$, where the substitutional Li impurity Li^x_{Mg} accepts a valence band electron leading to the negatively ionized Li'_{Mg} species and creating a hole $h^\bullet$ in the same band.

The interstitial Li insertion in the MgH_2 lattice can be described by the defect formation reaction $Li + V^x_i = Li^x_i$, where V^x_i is a vacant interstitial site and Li^x_i represents the same interstitial site filled by a Li atom. This process leads to an intercalated phase Li_xMgH_2. The calculated DFEs fall in the range 94.4−125.4 kJ/mol. It should be noted that the insertion of Li atoms in interstitial positions is not coupled to the removal of atoms from the sublattice of the original MgH_2 structure lattice and the formation of other reaction products. Thus, the energetics of the process is driven only by the ability of the host lattice to accommodate extrinsic species. In the case of MgH_2, this is permitted by the presence of an empty 1-D channel along the [001] direction in which the Li atoms can be accommodated. However, the filling of interstitial positions in the MgH_2 lattice by Li atoms leads to an increase in the internal stress of the cell that leads to a marked volume expansion. Interstitial Li atoms have been inserted in the 1-D channels of the MgH_2 structure, in the (0.5, 0, 0.5) fractional coordinate of the MgH_2 elementary cell. Further calculations have also been performed putting Li atoms in the positions described by (0.5, 0.5, 0.0) and (0.5, 0, z) fractional coordinates, with the z fractional site ranging between (−0.25 and 0.25). Only highly unstable systems have been obtained and have been therefore discarded. In the final relaxed Li_xMgH_2 lattice, Li ions are coordinated by a distorted octahedra with Li−H bond lengths spreading in the range of 1.77−2.00 Å. The electronic DOS shows clearly the presence of donor levels at the bottom of the conduction band which could easily be ionized, thus allowing an increase of n-type carrier concentration, by the ionization process $Li_i = Li_i + e'$, where the interstitial neutral Li_i atom ionizes to give a positive Li_i atom and a conduction electron.

The substitution of the H atom in the MgH_2 lattice by a Li atom according to the reaction $Li + H^x_H = Li^x_H + H_S$ leads to the Li_xMgH_{2-x} system. It is characterized by disorder in the anionic sublattice. The DFEs range between 331.9 and 348.0 kJ/mol, suggesting that this process of insertion is highly unfavorable. The Li ion in the H site leads to a notable distortion of the original coordination octahedra. Moreover, it also affects the volume of the overall MgH_2 unit cell, leading to a large expansion. The electronic DOS shows the presence of two spin symmetrical localized states in proximity of the bottom of the conduction band: occupied and unoccupied states are separated by ≈0.3 eV.

The last defective system $Li_xMg_{1-x}H_{2-x}$ is a doubly disordered lattice on both the cationic and anionic sublattices: a Li atom in a Mg site and H vacancy. Differently from the previous defective systems, this double defective supercell leads to an ensemble of inequivalent configurations. A systematic study of energies of $Li_xMg_{1-x}H_{2-x}$ systems with inequivalent H vacancies has been carried out in the 2 × 2 × 3 supercell, by fixing the substitutional Li atom in a Mg site: 12 nonequivalent H vacancy positions have been computed. The energy spectra of these defective systems have been found to be in perfect agreement with the previous work by Smith et al.[12] The most

dx.doi.org/10.1021/jp404993z | J. Phys. Chem. C 2013, 117, 22467−22477

Table 5. Calculated $\Delta_r E$ and $\Delta_r G(300\ K)$ of Reactions R4−R8 in the Three Supercells: Values Are Reported Per Mole of MgH_2[a]

reaction	$\Delta_r E$ (kJ/mol)	$\Delta_r G(300\ K)$ (kJ/mol)	ΔV %
$xLi + MgH_2 \rightarrow MgH_{2-x} + xLiH$ (R4)			
2 × 2 × 2	3.2	2.7	+0.03
2 × 2 × 3	2.1	1.7	+0.02
3 × 3 × 4	0.7	0.6	+0.01
$xLi + MgH_2 \rightarrow Li_xMg_{1-x}H_2 + xMg$ (R5)			
2 × 2 × 2	14.4	14.0	−0.51
2 × 2 × 3	9.2	8.9	−0.29
3 × 3 × 4	3.2	3.1	−0.07
$xLi + MgH_2 \rightarrow Li_xMgH_2$ (R6)			
2 × 2 × 2	7.8	7.4	+2.06
2 × 2 × 3	4.5	4.2	+1.53
3 × 3 × 4	1.3	1.2	+0.58
$2xLi + MgH_2 \rightarrow Li_xMgH_{2-x} + xLiH$ (R7)			
2 × 2 × 2	15.5	14.9	+4.08
2 × 2 × 3	10.5	10.1	+2.60
3 × 3 × 4	3.7	3.5	+0.88
$2xLi + MgH_2 \rightarrow Li_xMg_{1-x}H_{2-x} + xMg + xLiH$ (R8)			
2 × 2 × 2	−0.7	−1.4	+0.23
2 × 2 × 3	−0.4	−0.9	+0.14
3 × 3 × 4	−0.2	−0.4	+0.04

[a]Percentual volume changes of defective supercell compared to the perfect MgH_2 supercell are also reported.

stable configuration of the pair defects in the $Li_xMg_{1-x}H_{2-x}$ system is the close coupling in vicinal positions of the substitutional Li and the H vacancy. In light of these results on the 2 × 2 × 3 supercell and the predictions by Smith et al.,[12] DFT calculations have been performed for the larger supercells only for the most stable configuration of defects. The double substitution leads to a decrease of the length of the Li−H bonds and of the vicinal H−Mg bonds to 1.80 and 1.87 Å, respectively. The DFEs predicted for this double defective lattice are the smaller among the defective structures considered, ranging between 72.5 and 73.4 kJ/mol. The analysis of the electronic DOS shows a limited electronic disorder induced by these coupled point defects: the occurrence of localized states is evident at the edges of the valence and conduction bands, whereas the Fermi energy shows negligible changes with respect to the pristine MgH_2 lattice. Only a slight decrease of the band gap value of about 0.3 eV is reported. The limited electronic disorder is due to the electronic compensation effect induced by the coupling of these two point defects. The defect creation reaction $Li_S + Mg^x_{Mg} + H^x_H = Li^x_{Mg} + V^x_H + Mg_S + H_S$, where the defect states could ionize as $Li^x_{Mg} + V^x_H = Li'_{Mg} + V_H + h^\bullet + e'$, highlights that the concomitant production of conduction electrons and valence holes in the system is present. This constraint leads to a minor electronic rearrangement of states in proximity of the band edges.

3.4. Li Incorporation Reactions. The predicted total energies of the optimized defective supercells allow us to calculate $\Delta_r E$ for reactions R4−R8. In Table 5 the electronic energy changes per unit of MgH_2 are reported for the three supercell sizes, together with the $\Delta_r G(300\ K)$ obtained by adding the configurational contributions to the corresponding $\Delta_r E$. Volume changes induced by defects with respect to those of the unaltered MgH_2 lattice are also reported.

Reactions R4, R5, R6, and R7 show positive energy changes, whereas R8 shows a $\Delta_r E < 0$. All reaction energies show monotonic trends in function of the defect concentrations x. As expected, larger energy changes have been found for systems with larger defect concentration. Focusing on R8, apparently the low DFEs for the $Li_xMg_{1-x}H_{2-x}$ lattice and the parallel nucleation of two bulk phases (e.g., Mg and LiH) drive the thermodynamics of R8 to negative values. It is important to mention that the configurational entropy further stabilizes the defective lattices at finite T (see Table 5). This effect decreases the $\Delta_r G°(300\ K)$ values compared to $\Delta_r E(0\ K)$ for all reactions R4−R8. The $\Delta_r E$ of the demixing reaction $Li_xMg_{1-x}H_{2-x} \rightarrow xLiH + (1-x)MgH_2$ has been calculated to study the stability of the double defective system with respect to the mechanical mixture of pure hydride phases MgH_2 and LiH. Predictions for the demixing reaction are −6.3, −4.1, and −1.8 kJ/mol of MgH_2 for 2 × 2 × 2, 2 × 2 × 3, and 3 × 3 × 4 supercells, respectively. These negative values suggest the thermodynamic instability of the double defective $Li_xMg_{1-x}H_{2-x}$ solid solution at any defect concentrations.[12]

It is worthy to recall that previous experimental observations[2] suggest a contraction of the MgH_2 lattice parameters upon lithium incorporation in electrochemical cells. Apparently all our predictions, reported in Table 5, disagree with this evidence, thus suggesting the need of a more complex explanation of this phenomenon.

In summary, from the analysis of calculated $\Delta_r G(300\ K)$ for reactions R4−R8, the reaction R8 comes out to be the only feasible elementary step which could play a role in the incorporation of Li in the first stages of the HCR conversion reaction. On the other hand, due to the thermodynamics instability of the double defective system involved in R8, the latter reaction cannot lead to an intermediate solid solution, although it still may represent a local elementary reactive step in the reaction mechanism.

3.5. Cluster Reactivity. The optimized structure of the $Mg_{31}H_{62}$ cluster shows a C_{2v} point symmetry and is shown in Figure 4.

dx.doi.org/10.1021/jp404993z | J. Phys. Chem. C 2013, 117, 22467−22477

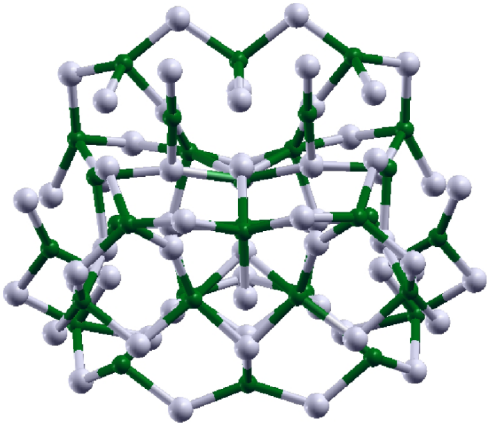

Figure 4. Equilibrium structure of the $Mg_{31}H_{62}$ (C_{2v}) cluster.

Mg atoms in the core of the cluster are coordinated by six H atoms in highly distorted octahedra with Mg−H bond lengths laying in a range 1.80−1.96 Å. On the contrary, Mg atoms on the surface are tetracoordinated by H atoms in tethraedra-like structures with bond lengths between 1.74 and 2.02 Å. The total energy per MgH_2 unit of the $Mg_{31}H_{62}$ cluster is larger than the bulk value of about 8%, indicating, as expected, a decrease of the thermodynamics stability of the nanosized MgH_2 due to surface effects.[18] The predicted potential in a lithium cell of the HCR process of the 1 nm $Mg_{31}H_{62}$ cluster is 0.9 V vs Li^+/Li, thus suggesting an increase of the working voltage of nano-MgH_2 compared to the bulk.

Defects have been modeled in the MgH_2 cluster following the same approach illustrated for the bulk systems (see section 3.3): point defects in the core of each cluster have been considered. DFEs of defective clusters have been calculated and compared with DFEs obtained for bulk systems: they are compared in the Figure 5.

The DFEs for the clusters show smaller values with respect to the bulk systems; in particular, a wide decrease is predicted for the defective clusters with disorder in the H sublattice. MgH_{2-x} and $Li_xMg_{1-x}H_{2-x}$ systems both show a negative DFE, indicating that at the nanoscale these two defective structures are energetically more stable than the unperturbed MgH_2 cluster.

Total energies of the defective clusters have been used to calculate the Δ_rE at 0 K for all the reactions R4−R8: the values are reported in Table 6, where reactions are relabeled

Table 6. Δ_rE of Reactions R4c−R8c in $Mg_{31}H_{62}$ Clusters: All Values Are Expressed Per Mole of MgH_2

reaction	$\Delta_rE^\circ_{el}$ (kJ/mol)
$Li + Mg_{31}H_{62} \rightarrow Mg_{31}H_{61} + LiH$ (R4c)	−8.04
$Li + Mg_{31}H_{62} \rightarrow LiMg_{30}H_{62} + Mg$ (R5c)	+4.14
$Li + Mg_{31}H_{62} \rightarrow LiMg_{31}H_{62}$ (R6c)	+0.80
$2Li + Mg_{31}H_{62} \rightarrow LiMg_{31}H_{61} + LiH$ (R7c)	−7.57
$2Li + Mg_{31}H_{62} \rightarrow LiMg_{30}H_{61} + Mg + LiH$ (R8c)	−13.76

R4c−R8c. The electronic energy values used for Mg, Li, and LiH are those of the bulk phases. Reactions R4c−R8c show all smaller or more negative Δ_rE values at the nanoscale with respect to the bulk reactions: reactions R4c, R7c, and R8c show negative Δ_rE values. In particular, the inversion of the Δ_rE values for the reaction R7c is remarkable: this reaction in the bulk phase shows the larger positive Δ_rE.

To evaluate the possible occurrence in the HCR process of the three defective clusters involved in reactions R4c, R7c, and R8c (i.e., $Mg_{31}H_{61}$, $LiMg_{31}H_{61}$, and $LiMg_{30}H_{61}$), the Δ_rE at 0 K for the corresponding demixing reactions into MgH_2, Mg, and LiH have been evaluated. The reactions considered are

$$Mg_{31}H_{61} = \frac{1}{2}Mg + \frac{30.5}{31}Mg_{31}H_{61} \quad \text{(R9c)}$$

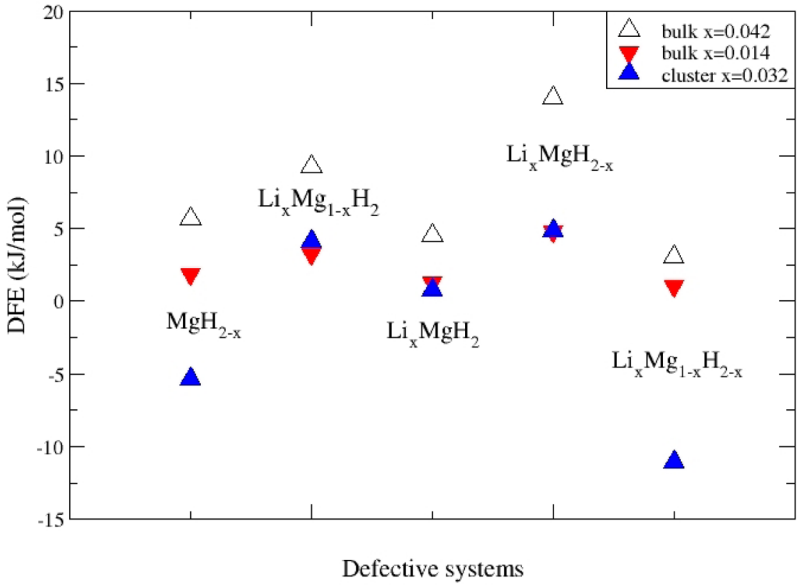

Figure 5. Calculated DFEs for bulk and cluster defective systems: all values are expressed per mole of MgH_2 for comparison. Bulk values refer to the DFEs calculated in the 2 × 2 × 3 and 3 × 3 × 4 supercells, corresponding to defect concentrations x of 0.042 and 0.014, respectively. Cluster DFE values are reported for the defective states of the $Mg_{31}H_{62}$ cluster: the relative concentration x is also reported.

dx.doi.org/10.1021/jp404993z | J. Phys. Chem. C 2013, 117, 22467−22477

$$LiMg_{31}H_{61} = Mg + LiH + \frac{30}{31}Mg_{31}H_{62} \quad \text{(R10c)}$$

$$LiMg_{30}H_{61} = LiH + \frac{30}{31}Mg_{31}H_{62} \quad \text{(R11c)}$$

All three, R9c, R10c, and R11c, reactions show positive $\Delta_r E$, i.e., 5.1, 2.0, and 8.1 kJ/mol MgH_2, respectively. This result is surprising and remarkable. In fact, it implies a drastic alteration of the overall HCR reaction thermodynamics. The three defective clusters are more stable compared to the corresponding demixed systems, thus suggesting that the overall HCR reaction sequence is very different at the nanoscale compared to the bulk. As a consequence, the formation of these solid solutions is thermodynamically favored in 1 nm clusters, and therefore they are predicted to be intermediate ground-state phases of the overall HCR process at the nanoscale. In general terms this behavior agrees with the well-known alteration of the high-temperature nano-MgH_2 desorption thermodynamics compared to the bulk.[15,27]

The solid solution formation sequence and extent is likely to be size dependent. Unfortunately, further detailed predictions are impossible starting from the here-reported data. However, from a qualitative point of view, our computational previsions suggest that nanosized MgH_2 particles undergo a more complex reaction path in lithium cells than the simple HCR.

As confirmed by experiments, bulk MgH_2 is unable to give HCR, while nanosized MgH_2 particles can undergoes this process.[1] The alteration of the reaction path at the nanoscale found by our DFT predictions may be the drive to the onset of the overall process on nanosized particles. Thus, in this case, "going-nano" allows the occurrence of the HCR process by a drastic alteration of the thermodynamics of the phases involved and not only by boosting the kinetics. It is important to mention that the results here presented are only preliminary, and larger computational efforts are needed to confirm our hypothesis (e.g., size of clusters, threshold of forces, thermodynamics at room temperature, etc). Further studies are in progress in our laboratories, and new extended results will be reported in future publications focused on the MgH_2 nanocluster reactivity in HCR.

4. CONCLUSION

In this study we reported a computational investigation of the MgH_2 conversion reaction to give Mg and LiH by first-principles methods. DFT calculations have been performed by investigating the occurrence of intermediate line compounds and solid solutions. The predicted MgH_2 HCR electrochemical potential is in excellent agreement with the experimental value, i.e., 0.53 V vs Li^+/Li at 300 K, to be compared with 0.5−0.55 V vs Li^+/Li in lithium cells. Apparently the HCR reaction sequence does not involve the formation of bulk intermediate phases: the $LiMgH_3$ and Li_2MgH_4 ternary compounds suggested by Chen and co-workers are apparently only metastable and are predicted to spontaneously demix to MgH_2 and LiH. Moreover, also the formation of solid solutions is thermodynamically unfavorable. Only the formation of a $Li_xMg_{1-x}H_{2-x}$ solid solution, where lithium atoms substitute magnesium and vicinal hydrogen vacancies occur, shows a negative $\Delta_r G(300\ K)$. However, also this solid solution spontaneously demixes to give MgH_2 and LiH. In this view it cannot be a reaction intermediate, and its formation may only be a local elementary reactive step in the overall reaction mechanism. On the contrary, the thermodynamics of the 1 nm MgH_2 nanoclusters, stoichiometric and defective, are strongly altered. Owing to this, the MgH_2 HCR thermodynamics is drastically altered in this nanosized system. In particular the formation of three different solid solutions (i.e., $Mg_{31}H_{61}$, $LiMg_{31}H_{61}$, and $LiMg_{30}H_{61}$) is thermodynamically favored in the 1 nm cluster, and therefore the HCR reaction sequence is necessarily altered at the nanoscale, compared to the bulk. Further studies are in progress in our laboratories, and new extended results will be reported in future publications focused on MgH_2 nanocluster reactivity.

■ ASSOCIATED CONTENT

Supporting Information

Tables S1, S2, and S3. This material is available free of charge via the Internet at http://pubs.acs.org.

■ AUTHOR INFORMATION

Corresponding Author

*E-mail: sergio.brutti@unibas.it.

Notes

The authors declare no competing financial interest.

■ ACKNOWLEDGMENTS

This study has been carried out in the framework of the Project "FIRB 2010 − Futuro in Ricerca: Idruri quali anodi ad alta capacità per batterie litio ione" (2012−2016), founded by the Italian Minister for University and Research (MIUR). The authors would like to thank the Caspur and the ISCRA-Cineca Consortia for the computational resources (Standard Computational Grant 2012 "MgH2 conversion reaction in Li-ion cells by first-principles method"; Class C project 2012-2013 "Ab initio study of MgH2 lithium incorporation").

■ REFERENCES

(1) Brutti, S.; Mulas, G.; Piciollo, E.; Panero, S.; Reale, P. *J. Mater. Chem.* **2012**, *22*, 14531.
(2) Oumellal, Y.; Rougier, A.; Nazri, G. A.; Tarascon, J. M.; Aymard, L. *Nat. Mater.* **2008**, *7*, 916.
(3) Oumellal, Y.; Rougier, A.; Tarascon, J. M.; Aymard, L. *J. Power Sources* **2009**, *192*, 698.
(4) Zaidi, W.; Oumellal, Y.; Bonnet, J.-P.; Zhang, J.; Cuevas, F.; Latroche, M.; Bobet, J.-L.; Aymard, L. *J. Power Sources* **2011**, *196*, 2854.
(5) Cabana, J.; Monconduit, L.; Larcher, D.; Palacin, M. R. *Adv. Mater.* **2010**, *22*, E170.
(6) Hassoun, J.; Croce, F.; Hong, I.; Scrosati, B. *Electrochem. Commun.* **2011**, *13*, 228.
(7) Boyanov, S.; Bernardi, J.; Bekaert, E.; Menetrier, M.; Doublet, M. L.; Monconduit, L. *Chem. Mater.* **2009**, *21*, 298−308.
(8) Ikeda, K.; Nakamori, Y.; Orimo, S. *Acta Mater.* **2005**, *53*, 3453.
(9) Li, D.; Zhang, T.; Yang, S.; Tao, Z.; Chen, J. *J. Alloys Compd.* **2011**, *509*, 8228.
(10) Pfrommer, B.; Elsasser, C.; Fahnle, M. *Phys. Rev. B* **1994**, *50*, 5089.
(11) Vajeeston, P.; Ravindran, P.; Kjekshus, A.; Fjellvag, H. *J. Alloys Compd.* **2008**, *450*, 327.
(12) Smith, K .C.; Fischer, T. S.; Waghmare, U. V.; Grau-Crespo, R. *Phys. Rev. B* **2010**, *82*, 134109.
(13) Wagemans, R. W. P.; Van Lenthe, J. H.; De Jongh, P. E.; Van Dillen, A. J.; De Jong, K. P. *J. Am. Chem. Soc.* **2005**, *127*, 16675.
(14) Wu, Z.; Allendorf, M. D.; Grossman, J. C. *J. Am. Chem. Soc.* **2009**, *131*, 13918.
(15) Aguey-Zinsour, K.-F.; Ares-Fernández, J.-R. *Chem. Mater.* **2008**, *20*, 376.

(16) Varin, R. A.; Czujko, T.; Wronski, Z. *Nanotechnology* **2006**, *17*, 3856.
(17) Schimmel, H. G.; Huot, J.; Chapon, L. C.; Tichelaar, F. D.; Mulder, F. M. *J. Am. Chem. Soc.* **2005**, *127*, 14348.
(18) Koukaras, E. N.; Zdetsis, A. D. *J. Am. Chem. Soc.* **2012**, *134*, 15914.
(19) Khatib, R.; Dalverny, A. L.; Saubanere, M.; Gaberscek, M.; Doublet, M. L. *J. Phys. Chem. C* **2013**, *117*, 837−849.
(20) Dalverny, A. L.; Filhol, J. S.; Doublet, M. L. *J. Mater. Chem.* **2011**, *21*, 10134.
(21) Kresse, G.; Furthmuller, J. *Comput. Mater. Sci.* **1996**, *6*, 15.
(22) Kresse, G.; Furthmuller, J. *Comput. Mater. Sci.* **1996**, *6*, 15; *Phys. Rev. B* **1996**, *54*, 11169. Kresse, G.; Hafner, J. *ibid.* **1993**, *48*, 13115; *J. Phys.: Condens. Matter* **1994**, *6*, 8245.
(23) Blochl, P. E. *Phys. Rev. B* **1994**, 17953.
(24) Perdew, J. P.; Chevary, J. A.; Vosko, S. H.; Jackson, K. A.; Pederson, M. R; Singh, D. J.; Fiolhais, C. *Phys. Rev. B* **1992**, *46*, 6671.
(25) Perdew, J. P.; Burke, K.; Ernzerhof, M. Generalized gradient approximation made simple. *Phys. Rev. Lett.* **1996**, *77*, 3865.
(26) Brutti, S.; Nguyen-Manh, D.; Pettifor, D. G. *Intermetallics* **2006**, *14* (12), 1472−1486.
(27) Isidorsson, J.; Giebels, I. E.; Arwin, H.; Griessen, R. *Phys. Rev. B* **2003**, *68*, 115112.
(28) Baroni, S.; Parravicini, G. P.; Pettica, G. *Phys. Rev. B* **1985**, *32*, 4077.
(29) Togo, A.; Oba, F.; Tanaka, I. *Phys. Rev. B* **2008**, *78*, 134106.
(30) Vosko, S. H.; Wilk, L.; Nusair, M. *Can. J. Phys.* **1980**, *58*, 1200.
(31) Van de Walle, C. G.; Neugebauer, J. *J. Appl. Phys.* **2004**, *95*, 3851.